# JGR Atmospheres

**Correspondence to:**

J. Chen and Z. Xie,
zqxie@ustc.edu.cn;
jbchen@tju.edu.cn

**Author Contributions:**
**Conceptualization:** Yue Qiu, Zhouqing Xie
**Formal analysis:** Yue Qiu
**Funding acquisition:** Jiubin Chen, Zhouqing Xie
**Investigation:** Yue Qiu, Pengxue Gai, Fange Yue, Yuanyuan Zhang, Pengzhen He
**Project Administration:** Jiubin Chen, Zhouqing Xie
**Resources:** Fange Yue, Pengzhen He, Hui Kang, Xiawei Yu
**Supervision:** Zhouqing Xie
**Visualization:** Yue Qiu, Xiawei Yu
**Writing – original draft:** Yue Qiu
**Writing – review & editing:** Paul K. S. Lam, Jiubin Chen, Zhouqing Xie

# Stable Mercury Isotopes Revealing Photochemical Processes in the Marine Boundary Layer

**Yue Qiu[1,2], Pengxue Gai[3], Fange Yue[1], Yuanyuan Zhang[4], Pengzhen He[1], Hui Kang[1], Xiawei Yu[1], Paul K. S. Lam[5], Jiubin Chen[3], and Zhouqing Xie[1,6]**

[1]Department of Environmental Science and Engineering, University of Science and Technology of China, Hefei, China, [2]Suzhou Institute for Advanced Study, University of Science and Technology of China, Suzhou, China, [3]Institute of Surface-Earth System Science, Tianjin University, Tianjin, China, [4]College of Resources and Environment, Chongqing School, University of Chinese Academy of Sciences, Chongqing, China, [5]Department of Chemistry, State Key Laboratory of Marine Pollution, City University of Hong Kong, Hong Kong, China, [6]Center for Excellence in Urban Atmospheric Environment, Institute of Urban Environment, Chinese Academy of Sciences, Xiamen, China

**Abstract** The marine boundary layer (MBL) is an important transportation and reaction zone of atmospheric mercury on Earth. However, the transformation mechanisms of Hg in the MBL remain unclear. In this study, total suspended particle samples were collected in the MBL during two cruises, and the levels of particulate bound mercury (PBM) and mercury isotopes were analyzed. The results showed that (a) continental anthropogenic emissions have limited contribution to PBM in the MBL; (b) PBM likely experienced the oxidation of $Hg^0$ by Br radicals and subsequent adsorption of $Hg^{2+}$ on to particulate surfaces, as inferred from the significant negative $\delta^{202}Hg$; (c) the $\Delta^{199}Hg/\Delta^{201}Hg$ ratio of ~1.0 suggests that PBM underwent photoreduction, which was influenced by organic compounds, and the contribution of photoreduction to the extent of odd-number mass-independent fractionation in PBM in the MBL was more significant than that of oxidation triggered by Br atoms. This study provides insights into the photochemical processes influencing mercury in the MBL.

## 1. Introduction

Atmospheric mercury (Hg) can be operationally defined into three types: gaseous elemental Hg (GEM), gaseous oxidized Hg (GOM), and particle-bound Hg (PBM). GEM is the most abundant Hg species in the global atmosphere (approximately 90%) and is well mixed due to its prolonged lifetime (0.5–1 year) and stable chemical properties. As GOM and PBM are more soluble in water than GEM and have a shorter lifetime (days to weeks), they are the predominant Hg species deposited to ecosystems through wet and dry deposition (Selin, 2009). The mutual transformations between these three Hg species have an important influence on the transportation and deposition of atmospheric Hg on a global scale (Schroeder & Munthe, 1998). The marine boundary layer (MBL) represents the atmospheric area affected by the oceanic surface, and its height significantly varies between middle–high latitudes (dozens to hundreds of meters) and low latitudes (up to 2000 m) (Hedgecock et al., 2005). The circulation of atmospheric Hg in the MBL differs from that in the planetary boundary layer (PBL) because of the significant differences in meteorological conditions and chemical compositions between the MBL and the PBL (e.g., humidity, sea salt aerosols, and oxidation mechanisms) (Jiang et al., 2021; Malcolm et al., 2010; Sigler et al., 2009; Timonen et al., 2013; Ye et al., 2016). As the MBL has relatively high humidity, sufficient sunlight, and abundant atmospheric oxidants, transformations among the three Hg species occur frequently (Hedgecock & Pirrone, 2001, 2004; Laurier et al., 2003; Sprovieri et al., 2010).

Previous studies have shown that atmospheric photochemical redox reactions have an important effect on the chemical transformation between these three Hg species in the atmosphere (Angot et al., 2016; Huang et al., 2019; Schroeder et al., 1998; Song et al., 2018). The importance of Br atoms in the $Hg^0$ oxidation was first recognized in previous studies to explain atmospheric $Hg^0$ depletion events occurring in the Arctic boundary layer during spring, as the photochemical reactions of sea salts supply a large amount of Br (Schroeder et al., 1998). The mechanism of $Hg^0$ oxidation by atomic Br is a two-stage exothermic reaction, in which $Hg^+$ is converted to $Hg^{2+}$ in the second stage via free radical oxidants (Balabanov & Peterson, 2003; Dibble et al., 2012; Donohoue et al., 2005, 2006; Goodsite et al., 2004). In addition, intermediates (HgBr)

formed in the first stage may be reduced back to $Hg^0$ by dissociation because of its thermal instability, which is a reaction considered to compete with oxidation (Balabanov & Peterson, 2003). Holmes et al. (2006) first proposed that atomic Br is the main oxidant for $Hg^0$. Recent background observations of tropospheric BrO indicate that Br-radical chemistry occurs widely in the troposphere (Theys et al., 2011; S. Wang, Schmidt, et al., 2015). Recent aircraft observations of $Hg^{2+}$ and BrO in the southeastern United States indicate that atomic Br is the main oxidant of $Hg^0$ (Gratz et al., 2015; Shah et al., 2016). Although there are numerous oxidants in the MBL, their contributions to the multiple redox transformations of atmospheric Hg are still unclear. A recent study revealed that although atomic Br may not be the direct oxidant for the generation of $Hg^{2+}$ on particulate surfaces in the MBL, it is likely the primary direct oxidant for the generation of GOMs (Yu et al., 2020). Photochemical reduction in aquatic systems has been widely observed in previous studies (Amyot et al., 2000; Costa & Liss, 1999; Mason et al., 2001). Moreover, research suggests that $Hg^{2+}$ first combines with dissolved organic carbon (DOC) or other organic matter (sulfur compound/carboxyl ligands) forming complexes during photochemical reduction, and the subsequent excitation of the complexes by sunlight leads to ligand-to-metal charge transfer inside the complexes, resulting in the reduction of $Hg^{2+}$ (Zheng & Hintelmann, 2009, 2010; Zheng et al., 2012). This process also occurs in organic aerosols. Recent studies have shown that the photoreduction of atmospheric GOM is underestimated in global Hg models, highlighting the importance of understanding the morphological distribution patterns of atmospheric Hg (Saiz-Lopez et al., 2018). Therefore, to date, the mechanisms through which atmospheric Hg species (especially PBM) undergo transformations in the MBL remain complex and unknown.

Stable Hg isotopes can be used to explore the sources and environmental processes of PBM. According to previous studies, several physical (e.g., mixing of plumes, evaporation and dissolution in droplets, diffusion, and adsorption and desorption on particulate surfaces) and chemical (e.g., photoreduction, gas-phase oxidation, and photodemethylation) processes can induce fractionation of Hg isotopes (Bergquist & Blum, 2007; Blum et al., 2014; Estrade et al., 2009; Fu et al., 2019; G. Sun et al., 2016; van Groos et al., 2014). There are typically three types of fractionation processes of Hg isotopes based on the fractionation characteristics and mass number of isotopes: mass-dependent fractionation (MDF, $\delta^{202}Hg$), odd-number mass-independent fractionation (odd-MIF, $\Delta^{199}Hg$, and $\Delta^{201}Hg$), and even-number mass-independent fractionation (even-MIF, $\Delta^{200}Hg$, and $\Delta^{204}Hg$). Previous studies have revealed that odd-MIF can be used to diagnose the occurrence of photoreduction, whereas even-MIF is a good indicator of Hg from the upper atmosphere or long-range transport (Bergquist & Blum, 2007; Chen et al., 2012; Enrico et al., 2016; Huang et al., 2019). To date, only a few studies have explored the isotopic fractionation mechanisms of atmospheric $Hg^0$ oxidation. G. Sun et al. (2016) demonstrated that the gas-phase oxidation of $Hg^0$ caused by Br and Cl atoms leads to negative $\Delta^{199}Hg$ and $\Delta^{201}Hg$ (triggered by the nuclear volume effect [NVE]) in the product $Hg^{2+}$. Owing to the short atmospheric residence time of PBM (typically a few days to a few weeks), Hg isotopes can be used to explore short-term atmospheric cycling of PBM in anthropogenic emissions from urban areas.

Previous studies have attempted exploring the atmospheric processes influencing PBM in the MBL through the isotopic characteristics in samples collected from coastal sites (Demers et al., 2015; Fu et al., 2018, 2019; Rolison et al., 2013; Yu et al., 2016). Coastal PBM samples are largely affected by anthropogenic emissions; hence, their isotopic characteristics record the signatures from both MBL atmospheric processes and anthropogenic emissions (Demers et al., 2015; Fu et al., 2018, 2019; Rolison et al., 2013; Yu et al., 2016). Therefore, cruise sampling (off the coast) can more effectively determine the atmospheric processes influencing PBM in the MBL relative to onshore sampling (Yu et al., 2020).

The objective of this study was to explore the atmospheric processes in the MBL that influence the isotopic characteristics of PBM by analyzing the samples collected during two research cruises. This study provides an understanding of the transformation mechanisms and spatial distribution patterns of atmospheric Hg in the MBL.

## 2. Materials and Methods

### 2.1. Sampling Locations and Sample Collection

The locations of the sampling sites are shown in Figure 1. Total suspended particle (TSP) samples were collected onboard the Xuelong research vessel during the 33rd Chinese Antarctic Research Expedition
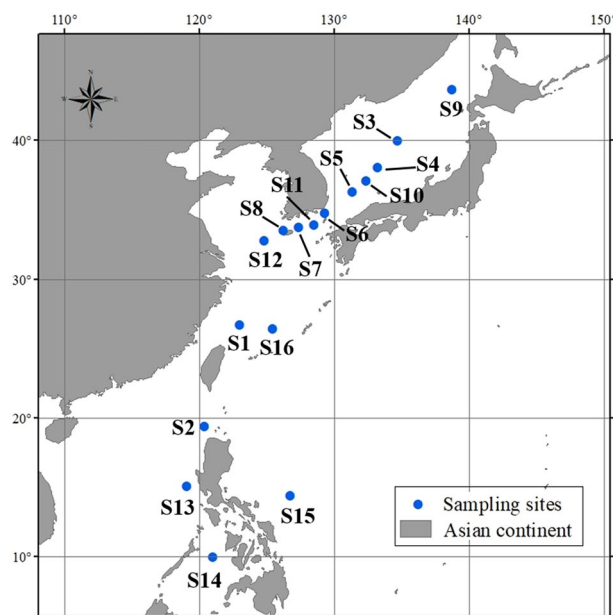
**Figure 1.** Distribution of sampling locations. The blue spots represent the locations at the "midpoint" moment during the sampling time of total suspended particles samples.

and the seventh Chinese Arctic Research Expedition in 2016. Additional details on the sampling time and corresponding weather data for each TSP sample are provided in Tables S1 and S2, respectively (see supplementary materials). In this study, 16 TSP samples were collected using two high-volume air samplers (Wuhan Tianhong Instrument Co., Ltd.) equipped with pre-combusted (450°C for 6 h) quartz fiber filters (quartz microfiber filters, 203 × 254 mm, 25 sheets, CAT No. 1851-865, Lot No. 9730862, UK), which collected particles at a flow rate of 1.05 m$^3$ min$^{-1}$. The collected TSP samples were then stored in a freezer at −4°C.

### 2.2. Hg Concentration and Isotope Analysis

Considering the low Hg content in the TSP samples due to the significant contribution of marine air masses, 12 and 24-h TSP samples collected in the MBL at the same period in the same location were composited to fulfill the detection limit of the isotope test (Table S1). Each composite TSP sample was pretreated employing the method described by Huang et al. (2015). The trapping solution, containing Hg, of each TSP sample was obtained after pretreatment. The pretreated trapping solutions were used to measure the content and isotopic ratios of Hg. We determined the Hg content of each TSP sample using a Tekran 2500 monitor (Model 2500 Cold Vapor Atomic Fluorescence Spectrophotometry detector, Tekran Instruments) according to the EPA Method 1631 Revision E. Eleven procedural blanks (the Hg amount in gold capture tubes were treated by the same procedures as in the sample determination), two sampling blanks (the Hg amount in quartz fiber filters, which were sampled for 1 min during non-haze days), and three certified reference materials (GSS-5 [yellow-red soil], Trace Metals–Loamy Sand 1, and GSD-11 [stream sediments]) were added to the test batch for quality control. The results showed that the average Hg amount in the procedural blanks ($n = 11$) was 1.15 ± 0.91 pg (mean ± 2 SD), which was not more than 0.7‰ of the Hg amount in each TSP sample. Moreover, the average Hg amount in the sampling blanks ($n = 2$) was 0.12 ± 0.04 ng (mean ± 2 SD), which was not more than 6% of the Hg amount in each TSP sample. The recovery of the Hg content in each TSP sample was represented by the recovery of the three certified reference materials, which ranged from 88% to 97% ($n = 6$) (Table S3). After calculation, we concluded that the effect of the sample matrix on the estimation of Hg isotope was negligible. The detailed calculations are presented in the supplementary materials (Table S4).

In this study, five Hg isotopes (including $^{198}$Hg, $^{199}$Hg, $^{200}$Hg, $^{201}$Hg, and $^{202}$Hg) from each TSP sample were determined using an MC-ICP-MS (Neptune Plus, ThermoFisher). Additional details of the analytical procedures and instrumental parameter settings were obtained from previous studies (Huang et al., 2015; Z. Wang, Chen, et al., 2015; Yuan et al., 2015).

The MDF of Hg isotopes was reported using the delta notation (δ) in units of per mil, referenced to the bracketed NIST 3133 Hg standard, which can be expressed as follows:

$$\delta^{\text{xxx}}\text{Hg}\,(\text{‰}) = \left(\left[\left(^{\text{xxx}}\text{Hg}/^{198}\text{Hg}\right)_{\text{sample}} \Big/ \left(^{\text{xxx}}\text{Hg}/^{198}\text{Hg}\right)_{\text{NIST3133}}\right] - 1\right) \times 1000$$

where xxx = 199, 200, 201, and 202. Any isotope composition that did not follow the theoretical MDF was considered an isotope anomaly caused by MIF. MIF values are indicated by "capital delta [Δ]" notation (per mil) and are predicted from δ$^{202}$Hg using the MDF law:

$$\Delta^{\text{xxx}}\text{Hg} = \delta^{\text{xxx}}\text{Hg} - \beta^{\text{xxx}} \times \delta^{202}\text{Hg}$$

where the mass-dependent scaling factor βxxx is 0.252 for $^{199}$Hg, 0.502 for $^{200}$Hg, and 0.752 for $^{201}$Hg.

For quality assurance and control, the measurements of secondary standard NIST SRM 3177 Hg were performed multiple times during each sample analysis session. The results showed average δ$^{202}$Hg, Δ$^{199}$Hg,

$\Delta^{200}$Hg, and $\Delta^{201}$Hg values of $-0.52‰ \pm 0.14‰$, $0.02‰ \pm 0.10‰$, $0.04‰ \pm 0.09‰$, and $0.00‰ \pm 0.09‰$, respectively (2 SD, $n = 10$). As the reference material UM-Almaden is no longer being produced and the Hg isotopic compositions of UM-Almaden and NIST SRM 3177 Hg were strictly the same, we compared our measurement data of NIST SRM 3177 Hg with those from previous studies (Bergquist & Blum, 2007; Chen et al., 2010; Huang et al., 2015, 2016, 2019) and found the values to be consistent. Each sample was only measured once as the available sample amount was limited. Therefore, we used the uncertainty of the Hg isotopes of NIST SRM 3177 Hg to represent the uncertainty of the isotopic composition of the aerosol samples. The measurement data are listed in Table S5.

### 2.3. Auxiliary Data Analysis

#### 2.3.1. Organic Carbon/Elemental Carbon (OC/EC)

OC and EC are important components of particles that can affect their physical and chemical properties (Archer & Blum, 2018). In this study, the OC and EC contents in each TSP sample were estimated using a multiwavelength carbon analyzer (DRI Model 2015, Desert Research Institute). The measurement data are presented in Table S6.

#### 2.3.2. Heavy Metal Elements

Previous studies have reported that continental anthropogenic emissions have an important influence on PBM collected at coastal sites and offshore boundary layers (Demers et al., 2015; Fu et al., 2018, 2019; Rolison et al., 2013; Yu et al., 2016, 2020). Therefore, the contents of eight heavy metals (Cd, Co, Cr, Cu, Mn, Ni, Pb, and Zn) in each TSP sample were measured using an ICP-MS (NexION 2000C, PerkinElmer) to estimate the contributions of continental anthropogenic emissions to PBM. The digestion method for each TSP sample and the corresponding quality control are presented in Text S1 and Table S7, respectively. The measurement data are presented in Table S6.

#### 2.3.3. Air-Mass Backward Trajectory Analysis

TrajStat, a geographical information system-based software, and gridded meteorological data (Global Data Assimilation System, GDAS1) from the U.S. National Oceanic and Atmospheric Administration were used to calculate 120-h backward trajectories of air masses arriving at a height of 50 m above sea level every 1 h during the sampling period on the two cruises. The continental cumulative anthropogenic PBM emission (continental anthropogenic $\sum$PBM emission) of each TSP sample was calculated by summing up all the gridded emissions of the grids encountered by the air mass transported during the past 5 days, based on the Arctic Monitoring and Assessment Program (AMAP)/United Nations Environment Program (UNEP) gridded PBM emission inventory for 2010 (AMAP/UNEP, 2013; Fu et al., 2019). The fractional air mass residence times over oceanic regions (fractional ARTs over oceans) were defined as the percentages of ARTs over oceanic regions relative to the total ARTs, which were calculated for each sample regardless of trajectory height.

## 3. Results and Discussion

### 3.1. Influence of Continental Anthropogenic Contribution

According to the backward trajectory analysis in this study, air masses during the sampling period partly passed over the Asian Continent, indicating the potential contribution of continental anthropogenic emissions to PBM. Pb in particulate matter is considered to be derived from human activities (e.g., consumption of leaded gasoline and coal, mining and smelting, industrial uses, and waste incineration) (Flegal et al., 2013). There was no correlation between the Pb and PBM contents in this study, indicating that PBM was not predominantly affected by human activities. In addition, as EC is typically emitted from combustion sources and is chemically stable in the atmosphere, its content can be used to indicate combustion pollution (Jones & Muthuri, 1997). In this study, no correlation existed between EC and PBM contents, indicating that combustion emissions did not influence PBM.

Previous studies have compared δ202Hg and Δ199Hg to effectively identify emission sources (Chen et al., 2012, 2016). PBM in the MBL presented negative $\delta^{202}$Hg and positive $\Delta^{199}$Hg ($\delta^{202}$Hg $= -0.69 \pm 1.10‰$;
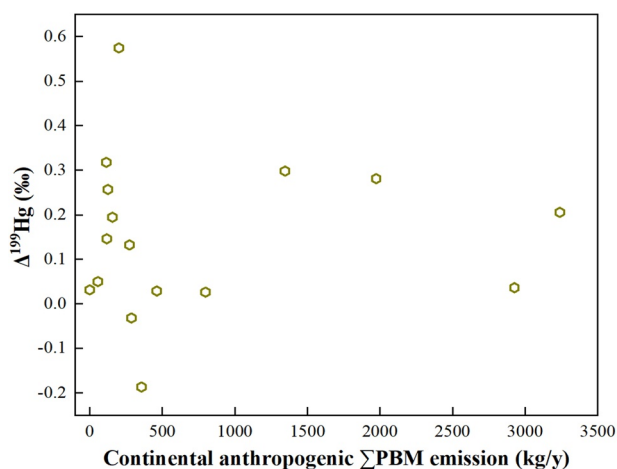
**Figure 2.** The correlation between continental anthropogenic particulate bound mercury (PBM) emissions (kg/y) and $\Delta^{199}$Hg (‰) in PBM of the marine boundary layer. The possible contribution of continental anthropogenic PBM emissions to PBM in each total suspended particle sample was calculated according to anthropogenic PBM emissions grid data published by AMAP/UNEP (2013).

$\Delta^{199}$Hg = 0.15 ± 0.18‰; mean ± 1 SD), which differed from the general isotopic compositions of PBM from anthropogenic emission sources (negative $\delta^{202}$Hg and negative $\Delta^{199}$Hg) (Huang et al., 2016); this suggests that anthropogenic emissions were not the main sources of PBM in the MBL. To clearly display the influence of anthropogenic emissions on PBM, we projected the 120-h air mass backward trajectory of each TSP sample. The amounts of PBM emissions at areas intersecting anthropogenic PBM emissions grid data from East Asia and backward trajectory of each TSP sample were extracted and summarized to ascertain possible contribution of anthropogenic emissions to PBM in each TSP sample. The data was then summarized to ascertain the possible contribution of anthropogenic emissions to PBM in each TSP sample. The results showed no correlation between continental anthropogenic emissions and $\Delta^{199}$Hg (Figure 2), further confirming the limited contribution of continental anthropogenic emissions to the PBM.

The average PBM content in this study was 9.64 ± 16.31 pg/m$^3$ (mean ± 1 SD), which was considerably lower than that in continental cities (including coastal cities). According to the PBM emission inventory in Eastern Asia, a variety of anthropogenic emission sources discharge significant amounts of PBM into the atmosphere. Therefore, the average PBM content collected from continental urban areas was considerably higher than that in the MBL because of the strong impact of anthropogenic emissions. In addition, the average PBM content in the MBL was lower than that in remote areas (e.g., mountainous areas) that are less affected by anthropogenic emissions. Moreover, the PBM contents measured in this study were lower than those reported in previous studies in the MBL (Table 1). This indicates that the differences in MBL conditions (e.g., temperature, humidity, and active substances) due to the differences in seasons and sampling locations can affect the PBM content.

**Table 1**

*Comparison of the Results of Atmospheric Particulate Bound Mercury Estimated in This Study With Those of Previous Studies*

| Study areas | Sample type | Sample size N | PBM (pg/m$^3$) Mean | 1 SD | References |
|---|---|---|---|---|---|
| An urban site in Guiyang, China | TSP | 15 | 214.67 | 100.20 | Yu et al., 2016 |
| An urban site in Guiyang, China | TSP | 11 | 442.73 | 199.80 | |
| A suburban industrialized area in Guiyang, China | TSP | 13 | 507.69 | 161.41 | |
| Dameishan atmospheric observatory, China | TSP | 7 | 342.86 | 102.10 | |
| A landfill site in Kolkata, India | PM$_{10}$ | 9 | 191.11 | 54.78 | Das et al., 2016 |
| A small industrial town in Kolkata, India | PM$_{10}$ | 16 | 280.94 | 107.02 | |
| A traffic junction in Kolkata, India | PM$_{10}$ | 27 | 393.33 | 78.02 | |
| An urban site in Xi'an, China | TSP | 69 | 640.41 | 541.24 | Xu et al., 2017 |
| Mt. Waliguan site in northwestern China | TSP | 25 | 84.48 | 41.13 | Fu et al., 2019 |
| Mt. Changbai site in northeastern China | TSP | 39 | 22.49 | 11.07 | |
| Mt. Ailao site in southwestern China | TSP | 36 | 31.37 | 29.15 | |
| Huaniao Island site in east China sea | TSP | 21 | 25.28 | 15.40 | |
| Marine boundary layer of offshore waters | TSP | 9 | 14.34 | 19.83 | Yu et al., 2020 |
| Marine boundary layer of offshore waters | TSP | 16 | 9.64 | 16.31 | This study |

Abbreviation: TSP, total suspended particles.
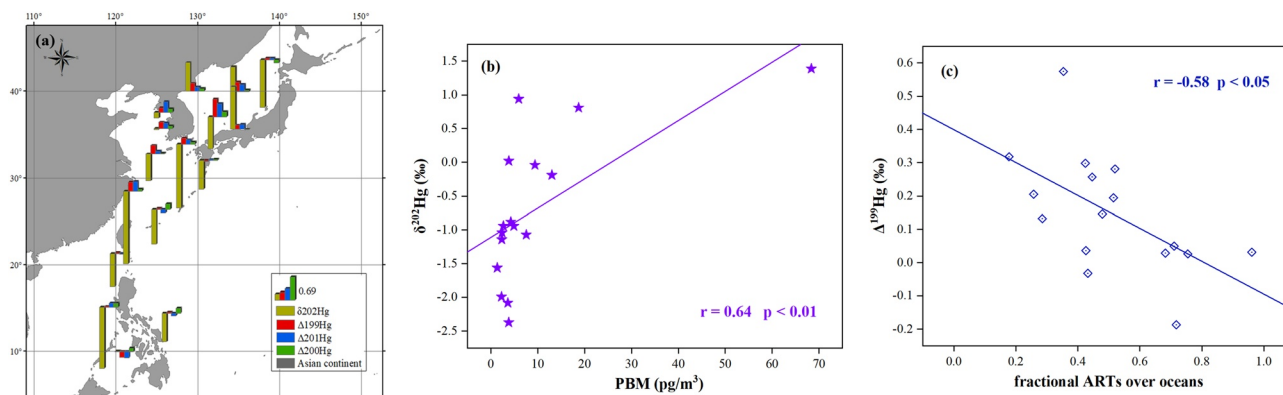
**Figure 3.** (a) The isotopic compositions of particulate bound mercury (PBM) collected in the marine boundary layer (MBL), including $\delta^{202}Hg$, $\Delta^{199}Hg$, $\Delta^{200}Hg$, and $\Delta^{201}Hg$ (‰); (b) Correlation between $\delta^{202}Hg$ and PBM content in total suspended particle (TSP) samples of the MBL; (c) Correlation between $\Delta^{199}Hg$ in PBM of the MBL and fractional ARTs over oceans for each TSP sample.

### 3.2. Impacts of Oxidation and Adsorption on PBM in the MBL: Evidence From $\delta^{202}Hg$ and $\Delta^{199}Hg$

Most of the samples exhibited significantly negative $\delta^{202}Hg$ values (Figure 3a), which is consistent with the reported values in PBM by previous studies (Fu et al., 2019; Huang et al., 2016, 2019; Yu et al., 2020). Previous studies have explored the physical and chemical processes that could induce negative $\delta^{202}Hg$ in PBM (Janssen et al., 2016; Smith et al., 2015; R. Sun et al., 2014, G. Sun et al., 2016; Wiederhold et al., 2010; L. Yang & Sturgeon, 2009; Zheng et al., 2007). Therefore, in this study, we subsequently discuss the impacts of potential physical and chemical processes on the negative $\delta^{202}Hg$ of PBM within the MBL.

PBM emitted by anthropogenic emissions typically has a negative $\delta^{202}Hg$ value. However, the discussion above suggests a limited contribution of direct emissions from continental anthropogenic activities to the PBM. This implies that anthropogenic emissions did not cause the significant negative $\delta^{202}Hg$ values in the PBM. According to previous studies, the ocean is an important reservoir of Hg, and the volatilization of dissolved gaseous Hg (primarily $Hg^0$) to the MBL is an important source of GEM (UN Environment, 2019); this process may lead to negative $\delta^{202}Hg$ in GEM, as the lighter Hg isotopes predominantly escape into the atmosphere (Zheng et al., 2007). However, the adsorption of GEM on particulate surfaces is limited compared to that of GOM (Yu et al., 2020), denying the oceanic volatilization as the main contributor to PBM.

The gas-phase oxidation of $Hg^0$ by Br/Cl atoms may partly explain the negative $\delta^{202}Hg$ in most PBM samples in this study. The fractionation of $^{202}Hg$ between the reactant ($Hg^0$) and product ($Hg^{2+}$) follows the Rayleigh fractionation, and the lighter Hg isotopes are commonly oxidized to $Hg^{2+}$ because of the kinetic isotope effect (G. Sun et al., 2016). This could trigger a negative $\delta^{202}Hg$ in $Hg^{2+}$ (the dominant Hg species in PBM) (Bergquist & Blum, 2007). However, during this oxidation process, the direction of $\delta^{202}Hg$ in GEM will gradually become positive, whereas that in PBM will gradually become more negative, thereby resulting in a relatively higher $\delta^{202}Hg$ in GEM than in PBM. The $\delta^{202}Hg$ of GEM in the MBL of the East China Sea (Fu et al., 2018) was not remarkably higher than the $\delta^{202}Hg$ values reported in this study (GEM: $-0.21 \pm 0.39$‰, PBM: $-0.69 \pm 1.10$‰, mean $\pm$ 1 SD). However, this phenomenon may be attributed to the inconsistency in spatiotemporal conditions during sample (GEM and PBM) collection. Another recent study analyzed the isotopic compositions of TGM (GEM + GOM) and PBM, which were collected under roughly the same spatiotemporal conditions (Yu et al., 2020). The $\delta^{202}Hg$ in the TGM was conspicuously higher than that in PBM (TGM: $-0.09 \pm 0.48$‰, PBM: $-0.80 \pm 0.58$‰, mean $\pm$ 1 SD). In addition, the variation range of $\delta^{202}Hg$ in PBM reported in this study was similar to that reported by Yu et al. (2020). These results may indicate the contribution of $Hg^0$ oxidation to PBM collected in this study. However, as we did not measure the isotopic composition of GEM collected under the same spatiotemporal conditions as PBM, this conclusion requires further confirmation through future studies.

In this study, a significant correlation was observed between PBM content and $\delta^{202}Hg$ ($r = 0.64$, $p < 0.01$) (Figure 3b), whereas the correlations between PBM content and the extent of odd-MIF were not significant ($p > 0.05$) (Figure S3). Therefore, we propose a mechanism for this phenomenon. Due to the occurrence

of oxidation processes (as previously mentioned), the PBM may have been impacted by multiple chemical mechanisms, resulting in the non-significant correlations between the extent of odd-MIF and PBM content in this study. Based on the correlation between $\Delta^{199}Hg$ and fractional ARTs over the oceans (Figure 3c), the $\Delta^{199}Hg$ in PBM exhibited a declining trend with increasing fractional ARTs over the oceans. Previous studies have shown that oxidation by Br radicals is the main oxidation pathway for GEM in MBL, and one study reported that the gas-phase oxidation of $Hg^0$ triggered by Br atoms would induce a negative odd-MIF in PBM (Holmes et al., 2006; Schroeder et al., 1998; G. Sun et al., 2016; Ye et al., 2016). This correlation may indicate the contribution of gas-phase oxidation of $Hg^0$ triggered by Br atoms in the MBL to PBM collected in this study. However, the $\Delta^{199}Hg$ in PBM was typically positive in this study ($0.15 \pm 0.18‰$, mean $\pm$ 1 SD), which may indicate the contributions of other chemical processes to PBM (e.g., oxidation of $Hg^0$ in the PBL and photoreduction). However, we observed a significant correlation between $\delta^{202}Hg$ and $PBM^{-1}$ in the TSP samples of the MBL (Figure 3b), suggesting a binary mixing of end-member sources, with one end-member characterized by elevated PBM content and moderately positive $\delta^{202}Hg_{PBM}$ and the other end-member characterized by low PBM content and significantly negative $\delta^{202}Hg_{PBM}$.

To date, no previous study has observed MIF in PBM during the adsorption process. Adsorption will lead to negative MDF in PBM because lighter Hg isotopes are predominantly adsorbed on to particulate surfaces. Hence, the oxidation of $Hg^0$ triggered by Br atoms and the adsorption of $Hg^{2+}$ on particulate surfaces significantly contributed to $\delta^{202}Hg$ in PBM.

### 3.3. Role of Photoreduction on PBM: Evidence From $\Delta^{199}Hg$ and $\Delta^{201}Hg$

Notably, three TSP samples exhibited extremely positive $\delta^{202}Hg$ in this study (S3: 0.81‰, S4: 1.39‰, S5: 0.94‰), likely indicating the contributions of other sources and/or processes to PBM in the MBL. Bergquist and Blum (2007) reported that the photoreduction of both inorganic $Hg^{2+}$ and MeHg induced a positive $\delta^{202}Hg$ in reactants due to isotopic fractionation followed by Rayleigh-type fractionation, which may indicate the strong impact of photoreduction on PBM in these three samples. Another study confirmed this finding, reporting higher $\delta^{202}Hg$ values during the day than during the previous or following nights in consecutive pairs of day–night $PM_{2.5}$ measurements, and the ratio of $\Delta^{199}Hg/\delta^{202}Hg$ was close to that of the photoreduction of $Hg^{2+}$ (Bergquist & Blum, 2007; Huang et al., 2019). Some processes that do not involve redox reactions, including the combination of $Hg^{2+}$ and mercaptan groups, ethylation of $Hg^{2+}$, precipitation of $Hg^{2+}$ (HgO/HgS), and production of MeHg by iron- and sulphate-reducing bacteria, can also induce MDF in $Hg^{2+}$ phases (Janssen et al., 2016; Smith et al., 2015; Wiederhold et al., 2010; L. Yang & Sturgeon, 2009). However, to date, the specific form of $Hg^{2+}$ on particle surfaces remains unknown, and therefore, the impacts of these processes on PBM in the MBL remain unclear.

$Hg^{2+}$ adsorbed on particulate surfaces may have experienced photoreduction. This is inferred from the ratio of $\Delta^{199}Hg/\Delta^{201}Hg$ derived from Hg emission sources with high $\Delta^{199}Hg$ and $\Delta^{201}Hg$ values (Blum et al., 2014). In this study, $\Delta^{199}Hg$ and $\Delta^{201}Hg$ in PBM exhibited a significant positive correlation ($r = 0.83$, $p < 0.001$), and $\Delta^{199}Hg/\Delta^{201}Hg$ was $0.86 \pm 0.16$ (Figure 4a), which was close to the value of 1.0 observed in the $Hg^{2+}$-photoreduction process in aqueous systems (Bergquist & Blum, 2007). As the photoreduction of $Hg^{2+}$ induces positive odd-MIF in residual $Hg^{2+}$, this atmospheric process may explain the positive $\Delta^{199}Hg$ and $\Delta^{199}Hg/\Delta^{201}Hg$ ($\sim$1.0) in the PBM in this study. Therefore, the photoreduction of PBM is likely a potential source of GEM in the atmosphere.

As shown in Figures 4b and 4c, the odd-MIF values in PBM in the MBL below 20°N were typically lower than those above 20°N, with the most negative odd-MIF value observed near 10°N. Moreover, it was found that TSP samples collected above 20°N seemed to be close to the high $Hg^{2+}$ emission regions, while which collected below 20°N were located in open sea. Considering the possible lowest reaction rate of photoreduction of PBM compared to that of gaseous and aqueous $Hg^{2+}$ (Saiz-Lopez et al., 2018; X. Yang et al., 2019), therefore, much more photoreduction of $Hg^{2+}$ in source regions before adsorption on particulate surfaces may be a reasonable explanation for this phenomenon. Studies suggest that during photochemical reduction, $Hg^{2+}$ first combines with DOC or other organic matter (sulfur compound/carboxyl ligands) forming complexes, and the excitation of the complexes by sunlight leads to ligand-to-metal charge transfer inside the complexes, resulting in the reduction of $Hg^{2+}$ (Zheng & Hintelmann, 2009, 2010; Zheng et al., 2012). Therefore, the photoreduction of $Hg^{2+}$ requires the participation of dissolved organic matter. Evidently, the
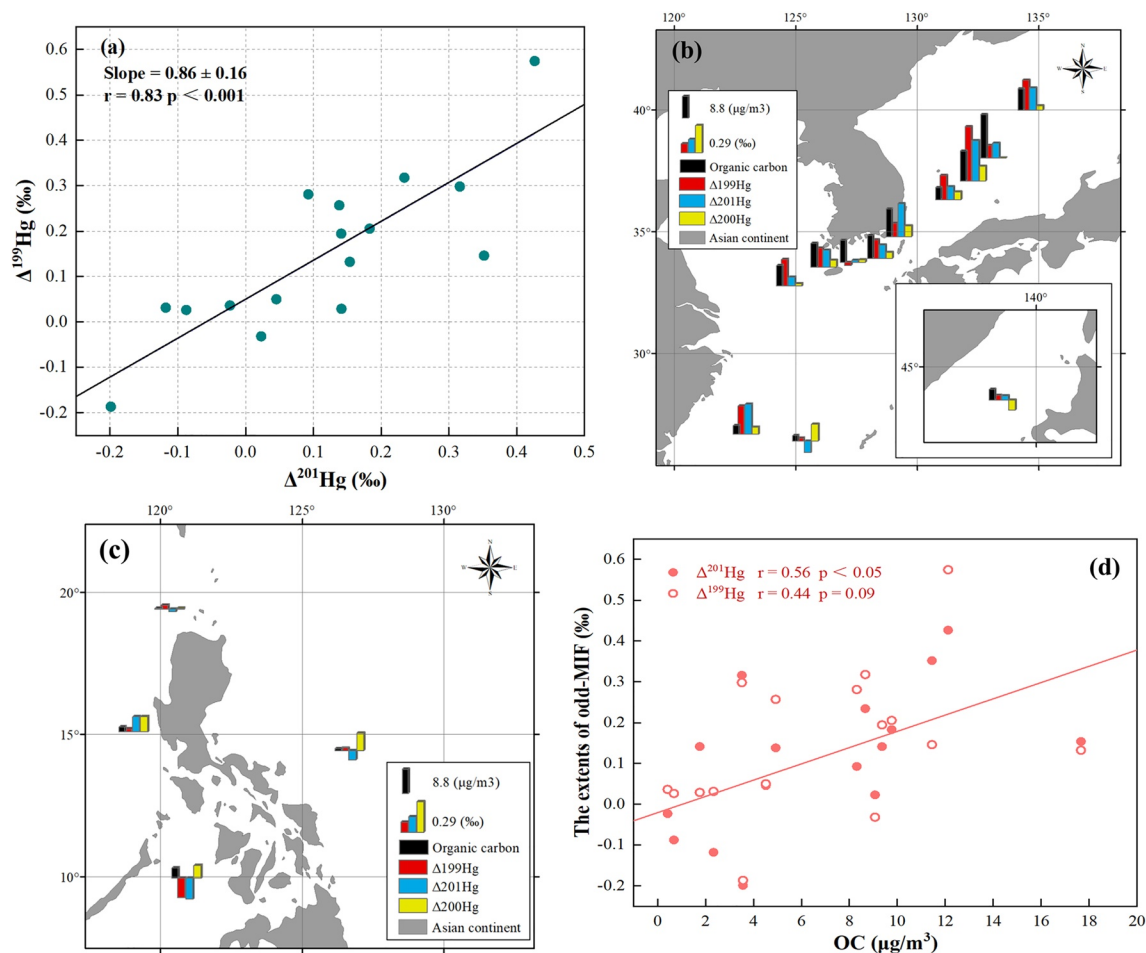
**Figure 4.** (a) Correlation between $\Delta^{199}$Hg and $\Delta^{201}$Hg in particulate bound mercury of the marine boundary layer (MBL); (b) The Hg isotopic compositions (‰) and organic carbon content ($\mu$g/m$^3$) in total suspended particle (TSP) collected above 20°N; (c) The Hg isotopic compositions (‰) and organic carbon content ($\mu$g/m$^3$) in TSP collected below 20°N; (d) The correlations between the extents of odd-MIF and OC content in TSP in the MBL.

latitudinal distribution of OC content on the particles in the MBL were similar to those of the odd-MIF values (Figures 4b and 4c). The OC content in TSP above 30°N MBL was significantly higher than that below 30°N MBL. This shows the importance of OC in the photoreduction of PBM. According to the correlations between the extent of odd-MIF and OC content in TSP in the MBL (Figure 4d), the positive correlation between $\Delta^{199}$Hg and OC content was non-significant ($r = 0.44$, $p = 0.09$); however, a significant positive correlation was observed between $\Delta^{201}$Hg and OC content ($r = 0.56$, $p < 0.05$), suggesting that the photoreduction of PBM was inhibited due to the lower OC content.

The ratio of $\Delta^{199}$Hg/$\Delta^{201}$Hg has been typically used in previous studies to identify specific photochemical reactions (Bergquist & Blum, 2007; G. Sun et al., 2016). $\Delta^{199}$Hg/$\Delta^{201}$Hg values of 1.00 and 1.36 indicate the photoreduction of Hg$^{2+}$ and MeHg, respectively, which is considered to be induced by the magnetic isotope effect (Bergquist & Blum, 2007). Moreover, $\Delta^{199}$Hg/$\Delta^{201}$Hg values of 1.64 and 1.89 indicate the gas-phase oxidation of Hg$^0$ triggered by Br and Cl atoms, respectively, in which the odd-MIF is considered to be induced by the nuclear volume effect (G. Sun et al., 2016). A previous analysis found that both oxidation and photoreduction may have contributed to the odd-MIF in PBM collected from the MBL. In this study, the $\Delta^{199}$Hg/$\Delta^{201}$Hg ratio in PBM was slightly <1.0 (Figure 4a); thus, based on the signatures of $\Delta^{199}$Hg/$\Delta^{201}$Hg induced by gas-phase oxidation and photoreduction, this value suggests that the contribution of Hg$^{2+}$ photoreduction to the extents of odd-MIF in PBM in the MBL is more significant than the contribution of gas-phase oxidation triggered by Br and Cl atoms.
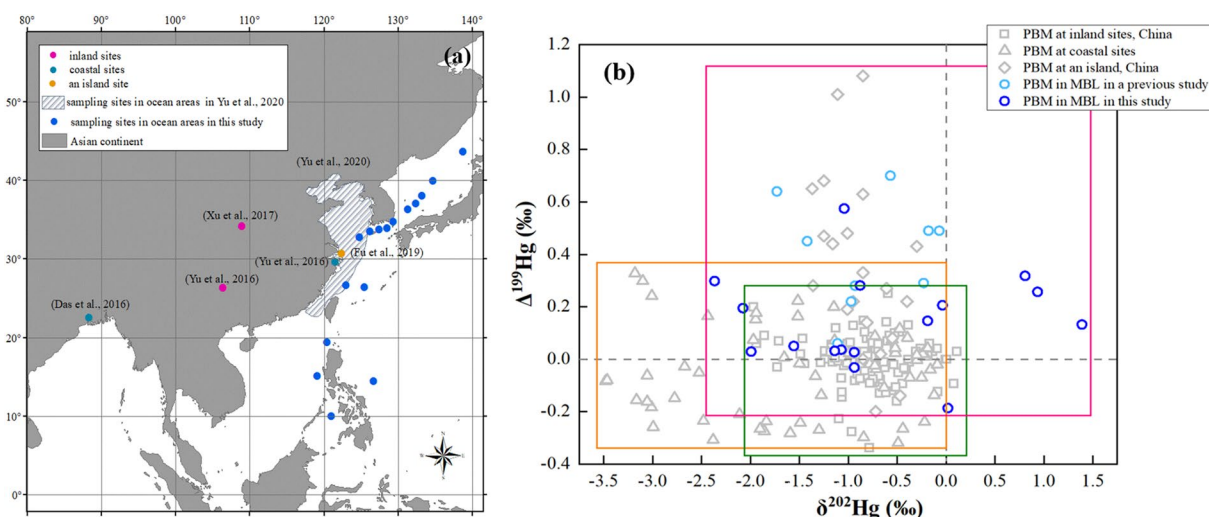
**Figure 5.** (a) The sampling locations at inland and coastal cities in East Asia and marine boundary layer (MBL);(b) The $\delta^{202}$Hg and $\Delta^{199}$Hg in particulate bound mercury collected in previous studies and this study. Gray hollow squares represent total suspended particle (TSP) collected at inland cities in China (Xu et al., 2017; Yu et al., 2016); gray hollow triangles represent TSP collected at coastal cities in East Asia (Das et al., 2016; Yu et al., 2016); gray hollow rhombi represent TSP collected at an island in China (Fu et al., 2019); light blue hollow circles represent TSP collected in the MBL in a previous case study (Yu et al., 2020); dark blue hollow circles represent TSP collected in the MBL in this study.

The above discussion suggests that PBM in the MBL may be influenced by both $Hg^0$ oxidation triggered by Br radicals and photoreduction influenced by organic compounds (e.g., OC). According to Figure 5, it shows significantly higher maximum $\Delta^{199}$Hg values in PBM of the MBL than that in inland and coastal sites. Considering that the PBM in the MBL may be influenced by both oxidation and photoreduction, and the contribution of photoreduction to the extent of odd-MIF in PBM in the MBL is more significant than that of oxidation, this may indicate the importance of oxidation and photoreduction in causing multiple chemical transformations and circulations during the long-distance transport of GEM in the MBL (Figure 6). This possibly explains the extremely positive $\Delta^{199}$Hg values in PBM in the MBL. However, as isotopic research on Hg species in the MBL is scarce, further studies are necessary to confirm this speculation.
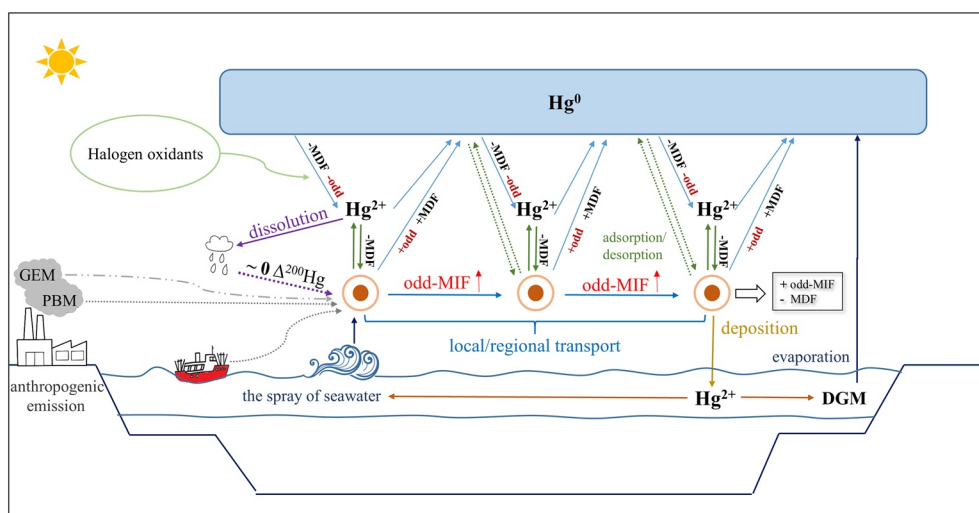


**Figure 6.** Schematic of the chemical processes undergone by mercury in the marine boundary layer. The solid lines represent processes that are known to exist, the dotted lines represent processes about which the contribution to particulate bound mercury is limited, and the dot–dash lines represent unknown processes.

## 4. Conclusions

This study explored the photochemical processes of Hg in the MBL through the analysis of Hg stable isotopes. The MBL is an appropriate zone for studying the atmospheric chemical processes of Hg, as it is negligibly affected by continental anthropogenic emissions. This study found that PBM may be contributed by oxidation and subsequent adsorption on to particles, and it may be affected by photoreduction. The results showed that the impact of photoreduction on the extent of odd-MIF in the PBM of the MBL was more significant than that of oxidation due to the $\Delta^{199}Hg/\Delta^{201}Hg$ ratio of ∼1.0 and the typically positive $\Delta^{199}Hg$ values (0.15 ± 0.18‰, mean ± 1 SD). Although this study provides valuable insights, the sample size was limited; therefore, further studies should be conducted to verify these conclusions.

## Data Availability Statement

This study complies with AGU data policy. The data is available in the Mendeley Data repository (http://dx.doi.org/10.17632/z48znmzfn8.1). The AMAP/UNEP gridded PBM emission inventory for 2010 are available from AMAP official website (https://www.amap.no/mercury-emissions/datasets).

## References

AMAP/UNEP (2013). Geospatially distributed mercury emissions dataset 2010, v1.

Amyot, M., Lean, D. R. S., Poissant, L., & Doyon, M. R. (2000). Distribution and transformation of elemental mercury in the St. Lawrence River and Lake Ontario. *Canadian Journal of Fisheries and Aquatic Sciences*, *57*, 155–163. https://doi.org/10.1139/cjfas-57-S1-15510.1139/f99-248

Angot, H., Dastoor, A., De Simone, F., Gardfeldt, K., Gencarelli, C. N., Hedgecock, I. M., et al. (2016). Chemical cycling and deposition of atmospheric mercury in polar regions: Review of recent measurements and comparison with models. *Atmospheric Chemistry and Physics*, *16*(16), 10735–10763. https://doi.org/10.5194/acp-16-10735-2016

Archer, D. E., & Blum, J. D. (2018). A model of mercury cycling and isotopic fractionation in the ocean. *Biogeosciences*, *15*(20), 6297–6313. https://doi.org/10.5194/bg-15-6297-2018

Balabanov, N. B., & Peterson, K. A. (2003). Mercury and reactive halogens: The thermochemistry of Hg+ {Cl-2, Br-2, BrCl, ClO, and BrO}. *Journal of Physical Chemistry A*, *107*(38), 7465–7470. https://doi.org/10.1021/jp035547p

Bergquist, B. A., & Blum, J. D. (2007). Mass-dependent and -independent fractionation of Hg isotopes by photoreduction in aquatic systems. *Science*, *318*(5849), 417–420. https://doi.org/10.1126/science.1148050

Blum, J. D., Sherman, L. S., & Johnson, M. W. (2014). Mercury isotopes in earth and environmental sciences. In R. Jeanloz (Ed.), *Annual Review of Earth and Planetary Sciences* (Vol. 42, pp. 249–269). Annual Reviews. https://doi.org/10.1146/annurev-earth-050212-124107

Chen, J., Hintelmann, H., & Dimock, B. (2010). Chromatographic pre-concentration of Hg from dilute aqueous solutions for isotopic measurement by MC-ICP-MS. *Journal of Analytical Atomic Spectrometry*, *25*(9), 1402–1409. https://doi.org/10.1039/c0ja00014k

Chen, J., Hintelmann, H., Feng, X., & Dimock, B. (2012). Unusual fractionation of both odd and even mercury isotopes in precipitation from Peterborough, ON, Canada. *Geochimica et Cosmochimica Acta*, *90*, 33–46. https://doi.org/10.1016/j.gca.2012.05.005

Chen, J., Hintelmann, H., Zheng, W., Feng, X., Cai, H., Wang, Z., et al. (2016). Isotopic evidence for distinct sources of mercury in lake waters and sediments. *Chemical Geology*, *426*, 33–44. https://doi.org/10.1016/j.chemgeo.2016.01.030

Costa, M., & Liss, P. S. (1999). Photoreduction of mercury in sea water and its possible implications for Hg-0 air-sea fluxes. *Marine Chemistry*, *68*(1–2), 87–95. https://doi.org/10.1016/s0304-4203(99)00067-5

Das, R., Wang, X., Khezri, B., Webster, R. D., Sikdar, P. K., & Datta, S. (2016). Mercury isotopes of atmospheric particle bound mercury for source apportionment study in urban Kolkata, India. *Elementa-Science of the Anthropocene*, *4*, 1–12. https://doi.org/10.12952/journal.elementa.000098

Demers, J. D., Sherman, L. S., Blum, J. D., Marsik, F. J., & Dvonch, J. T. (2015). Coupling atmospheric mercury isotope ratios and meteorology to identify sources of mercury impacting a coastal urban-industrial region near Pensacola, Florida, USA. *Global Biogeochemical Cycles*, *29*(10), 1689–1705. https://doi.org/10.1002/2015gb005146

Dibble, T. S., Zelie, M. J., & Mao, H. (2012). Thermodynamics of reactions of ClHg and BrHg radicals with atmospherically abundant free radicals. *Atmospheric Chemistry and Physics*, *12*(21), 10271–10279. https://doi.org/10.5194/acp-12-10271-2012

Donohoue, D. L., Bauer, D., Cossairt, B., & Hynes, A. J. (2006). Temperature and pressure dependent rate coefficients for the reaction of Hg with Br and the reaction of Br with Br: A pulsed laser photolysis-pulsed laser induced fluorescence study. *Journal of Physical Chemistry A*, *110*(21), 6623–6632. https://doi.org/10.1021/jp054688j

Donohoue, D. L., Bauer, D., & Hynes, A. J. (2005). Temperature and pressure dependent rate coefficients for the reaction of Hg with Cl and the reaction of Cl with Cl: A pulsed laser photolysis-pulsed laser induced fluorescence study. *Journal of Physical Chemistry A*, *109*(34), 7732–7741. https://doi.org/10.1021/jp051354l

Enrico, M., Le Roux, G., Maruszczak, N., Heimburger, L. E., Claustres, A., Fu, X., et al. (2016). Atmospheric mercury transfer to peat bogs dominated by gaseous elemental mercury dry deposition. *Environmental Science & Technology*, *50*(5), 2405–2412. https://doi.org/10.1021/acs.est.5b06058

Estrade, N., Carignan, J., Sonke, J. E., & Donard, O. F. X. (2009). Mercury isotope fractionation during liquid-vapor evaporation experiments. *Geochimica et Cosmochimica Acta*, *73*(10), 2693–2711. https://doi.org/10.1016/j.gca.2009.01.024

Flegal, A. R., Gallon, C., Ganguli, P. M., & Conaway, C. H. (2013). All the lead in China. *Critical Reviews in Environmental Science and Technology*, *43*(17), 1869–1944. https://doi.org/10.1080/10643389.2012.671738

Fu, X., Yang, X., Tan, Q., Ming, L., Lin, T., Che-Jen, L., et al. (2018). Isotopic composition of gaseous elemental mercury in the marine boundary layer of east China Sea. *Journal of Geophysical Research: Atmospheres*, *123*(14), 7656–7669. https://doi.org/10.1029/2018jd028671

Fu, X., Zhang, H., Feng, X., Tan, Q., Ming, L., Liu, C., & Zhang, L. (2019). Domestic and transboundary sources of atmospheric particulate bound mercury in remote areas of China: Evidence from mercury isotopes. *Environmental Science & Technology*, *53*(4), 1947–1957. https://doi.org/10.1021/acs.est.8b06736

Goodsite, M. E., Plane, J. M. C., & Skov, H. (2004). A theoretical study of the oxidation of Hg-0 to HgBr2 in the troposphere. *Environmental Science & Technology*, *38*(6), 1772–1776. https://doi.org/10.1021/es034680s

Gratz, L. E., Ambrose, J. L., Jaffe, D. A., Shah, V., Jaegle, L., Stutz, J., et al. (2015). Oxidation of mercury by bromine in the subtropical Pacific free troposphere. *Geophysical Research Letters*, *42*(23), 10494–10502. https://doi.org/10.1002/2015gl066645

Hedgecock, I. M., & Pirrone, N. (2001). Mercury and photochemistry in the marine boundary layer-modelling studies suggest the in situ production of reactive gas phase mercury. *Atmospheric Environment*, *35*(17), 3055–3062. https://doi.org/10.1016/s1352-2310(01)00109-1

Hedgecock, I. M., & Pirrone, N. (2004). Chasing quicksilver: Modeling the atmospheric lifetime of Hg-(g) (0) in the marine boundary layer at various latitudes. *Environmental Science & Technology*, *38*(1), 69–76. https://doi.org/10.1021/es034623z

Hedgecock, I. M., Trunfio, G. A., Pirrone, N., & Sprovieri, F. (2005). Mercury chemistry in the MBL: Mediterranean case and sensitivity studies using the AMCOTS (Atmospheric Mercury Chemistry over the Sea) model. *Atmospheric Environment*, *39*(38), 7217–7230. https://doi.org/10.1016/j.atmosenv.2005.09.002

Holmes, C. D., Jacob, D. J., & Yang, X. (2006). Global lifetime of elemental mercury against oxidation by atomic bromine in the free troposphere. *Geophysical Research Letters*, *33*(20), 5. https://doi.org/10.1029/2006gl027176

Huang, Q., Chen, J., Huang, W., Fu, P., Guinot, B., Feng, X., et al. (2016). Isotopic composition for source identification of mercury in atmospheric fine particles. *Atmospheric Chemistry and Physics*, *16*(18), 11773–11786. https://doi.org/10.5194/acp-16-11773-2016

Huang, Q., Chen, J., Huang, W., Reinfelder, J. R., Fu, P., Yuan, S., et al. (2019). Diel variation in mercury stable isotope ratios records photoreduction of PM2.5-bound mercury. *Atmospheric Chemistry and Physics*, *19*(1), 315–325. https://doi.org/10.5194/acp-19-315-2019

Huang, Q., Liu, Y., Chen, J., Feng, X., Huang, W., Yuan, S., et al. (2015). An improved dual-stage protocol to pre-concentrate mercury from airborne particles for precise isotopic measurement. *Journal of Analytical Atomic Spectrometry*, *30*(4), 957–966. https://doi.org/10.1039/c4ja00438h

Janssen, S. E., Schaefer, J. K., Barkay, T., & Reinfelder, J. R. (2016). Fractionation of mercury stable isotopes during microbial methylmercury production by iron- and sulfate-reducing bacteria. *Environmental Science & Technology*, *50*(15), 8077–8083. https://doi.org/10.1021/acs.est.6b00854

Jiang, B., Xie, Z., Lam, P. K. S., He, P., Yue, F., Wang, L., et al. (2021). Spatial and temporal distribution of sea salt aerosol mass concentrations in the marine boundary layer from the Arctic to the Antarctic. *Journal of Geophysical Research: Atmospheres*, *126*(6), e2020JD033892. https://doi.org/10.1029/2020JD033892

Jones, M. B., & Muthuri, F. M. (1997). Standing biomass and carbon distribution in a papyrus (Cyperus papyrus L) swamp on Lake Naivasha, Kenya. *Journal of Tropical Ecology*, *13*, 347–356. https://doi.org/10.1017/s0266467400010555

Laurier, F. J. G., Mason, R. P., Whalin, L., & Kato, S. (2003). Reactive gaseous mercury formation in the North Pacific Ocean's marine boundary layer: A potential role of halogen chemistry. *Journal of Geophysical Research*, *108*(D17), 4529. https://doi.org/10.1029/2003jd003625

Malcolm, E. G., Ford, A. C., Redding, T. A., Richardson, M. C., Strain, B. M., & Tetzner, S. W. (2010). Experimental investigation of the scavenging of gaseous mercury by sea salt aerosol. *Journal of Atmospheric Chemistry*, *63*(3), 221–234. https://doi.org/10.1007/s10874-010-9165-y

Mason, R. P., Lawson, N. M., & Sheu, G. R. (2001). Mercury in the Atlantic Ocean: Factors controlling air-sea exchange of mercury and its distribution in the upper waters. *Deep-Sea Research Part II-Topical Studies in Oceanography*, *48*(13), 2829–2853. https://doi.org/10.1016/s0967-0645(01)00020-0

Rolison, J. M., Landing, W. M., Luke, W., Cohen, M., & Salters, V. J. M. (2013). Isotopic composition of species-specific atmospheric Hg in a coastal environment. *Chemical Geology*, *336*, 37–49. https://doi.org/10.1016/j.chemgeo.2012.10.007

Saiz-Lopez, A., Sitkiewicz, S. P., Roca-Sanjuan, D., Oliva-Enrich, J. M., Davalos, J. Z., Notario, R., et al. (2018). Photoreduction of gaseous oxidized mercury changes global atmospheric mercury speciation, transport and deposition. *Nature Communications*, *9*, 9. https://doi.org/10.1038/s41467-018-07075-3

Schroeder, W. H., Anlauf, K. G., Barrie, L. A., Lu, J., Steffen, A., Schneeberger, D. R., & Berg, T. (1998). Arctic springtime depletion of mercury. *Nature*, *394*(6691), 331–332. https://doi.org/10.1038/28530

Schroeder, W. H., & Munthe, J. (1998). Atmospheric mercury - An overview. *Atmospheric Environment*, *32*(5), 809–822. https://doi.org/10.1016/s1352-2310(97)00293-8

Selin, N. E. (2009). Global biogeochemical cycling of mercury: A review. *Annual Review of Environment and Resources*, *34*, 43–63. https://doi.org/10.1146/annurev.environ.051308.084314

Shah, V., Jaegle, L., Gratz, L. E., Ambrose, J. L., Jaffe, D. A., Selin, N. E., et al. (2016). Origin of oxidized mercury in the summertime free troposphere over the southeastern US. *Atmospheric Chemistry and Physics*, *16*(3), 1511–1530. https://doi.org/10.5194/acp-16-1511-2016

Sigler, J. M., Mao, H., Sive, B. C., & Talbot, R. (2009). Oceanic influence on atmospheric mercury at coastal and inland sites: A springtime noreaster in New England. *Atmospheric Chemistry and Physics*, *9*(12), 4023–4030. https://doi.org/10.5194/acp-9-4023-2009

Smith, R. S., Wiederhold, J. G., & Kretzschmar, R. (2015). Mercury isotope fractionation during precipitation of metacinnabar (beta-HgS) and montroydite (HgO). *Environmental Science & Technology*, *49*(7), 4325–4334. https://doi.org/10.1021/acs.est.5b00409

Song, S., Angot, H., Selin, N. E., Gallee, H., Sprovieri, F., Pirrone, N., et al. (2018). Understanding mercury oxidation and air-snow exchange on the East Antarctic Plateau: A modeling study. *Atmospheric Chemistry and Physics*, *18*(21), 15825–15840. https://doi.org/10.5194/acp-18-15825-2018

Sprovieri, F., Hedgecock, I. M., & Pirrone, N. (2010). An investigation of the origins of reactive gaseous mercury in the Mediterranean marine boundary layer. *Atmospheric Chemistry and Physics*, *10*(8), 3985–3997. https://doi.org/10.5194/acp-10-3985-2010

Sun, G., Sommar, J., Feng, X., Lin, C., Ge, M., Wang, W., et al. (2016). Mass-dependent and -independent fractionation of mercury isotope during gas-phase oxidation of elemental mercury vapor by atomic Cl and Br. *Environmental Science & Technology*, *50*(17), 9232–9241. https://doi.org/10.1021/acs.est.6b01668

Sun, R., Sonke, J. E., Heimburger, L. E., Belkin, H. E., Liu, G., Shome, D., et al. (2014). Mercury stable isotope signatures of world coal deposits and historical coal combustion emissions. *Environmental Science & Technology*, *48*(13), 7660–7668. https://doi.org/10.1021/es501208a

Theys, N., Van Roozendael, M., Hendrick, F., Yang, X., De Smedt, I., Richter, A., et al. (2011). Global observations of tropospheric BrO columns using GOME-2 satellite data. *Atmospheric Chemistry and Physics*, *11*(4), 1791–1811. https://doi.org/10.5194/acp-11-1791-2011

Timonen, H., Ambrose, J. L., & Jaffe, D. A. (2013). Oxidation of elemental Hg in anthropogenic and marine airmasses. *Atmospheric Chemistry and Physics*, *13*(5), 2827–2836. https://doi.org/10.5194/acp-13-2827-2013

UN Environment (2019). *Global mercury assessment 2018, UN environment Programme, chemicals and health branch Geneva, Switzerland.* Last access 10 April 2019. Available at https://www.unenvironment.org/resources/publication/global-mercury-assessment-2018

van Groos, P. G. K., Esser, B. K., Williams, R. W., & Hunt, J. R. (2014). Isotope effect of mercury diffusion in air. *Environmental Science & Technology*, *48*(1), 227–233. https://doi.org/10.1021/es4033666

Wang, S., Schmidt, J. A., Baidar, S., Coburn, S., Dix, B., Koenig, T. K., et al. (2015). Active and widespread halogen chemistry in the tropical and subtropical free troposphere. *Proceedings of the National Academy of Sciences of the United States of America*, *112*(30), 9281–9286. https://doi.org/10.1073/pnas.1505142112

Wang, Z., Chen, J., Feng, X., Hintelmann, H., Yuan, S., Cai, H., et al. (2015). Mass-dependent and mass-independent fractionation of mercury isotopes in precipitation from Guiyang, SW China. *Comptes Rendus Geoscience*, *347*(7–8), 358–367. https://doi.org/10.1016/j.crte.2015.02.006

Wiederhold, J. G., Cramer, C. J., Daniel, K., Infante, I., Bourdon, B., & Kretzschmar, R. (2010). Equilibrium mercury isotope fractionation between dissolved Hg (II) species and thiol-bound Hg. *Environmental Science & Technology*, *44*(11), 4191–4197. https://doi.org/10.1021/es100205t

Xu, H., Sonke, J. E., Guinot, B., Fu, X., Sun, R., Lanzanova, A., et al. (2017). Seasonal and annual variations in atmospheric Hg and Pb isotopes in Xi'an, China. *Environmental Science & Technology*, *51*(7), 3759–3766. https://doi.org/10.1021/acs.est.6b06145

Yang, L., & Sturgeon, R. (2009). Isotopic fractionation of mercury induced by reduction and ethylation. *Analytical and Bioanalytical Chemistry*, *393*(1), 377–385. https://doi.org/10.1007/s00216-008-2348-6

Yang, X., Jiskra, M., & Sonke, J. E. (2019). Experimental rainwater divalent mercury speciation and photoreduction rates in the presence of halides and organic carbon. *The Science of the Total Environment*, *697*, 133821. https://doi.org/10.1016/j.scitotenv.2019.133821

Ye, Z., Mao, H., Lin, C., & Kim, S. Y. (2016). Investigation of processes controlling summertime gaseous elemental mercury oxidation at midlatitudinal marine, coastal, and inland sites. *Atmospheric Chemistry and Physics*, *16*(13), 8461–8478. https://doi.org/10.5194/acp-16-8461-2016

Yu, B., Fu, X., Yin, R., Zhang, H., Wang, X., Lin, C., et al. (2016). Isotopic composition of atmospheric mercury in China: New evidence for sources and transformation processes in air and in vegetation. *Environmental Science & Technology*, *50*(17), 9262–9269. https://doi.org/10.1021/acs.est.6b01782

Yu, B., Yang, L., Wang, L., Liu, H., Xiao, C., Liang, Y., et al. (2020). New evidence for atmospheric mercury transformations in the marine boundary layer from stable mercury isotopes. *Atmospheric Chemistry and Physics*, *20*(16), 9713–9723. https://doi.org/10.5194/acp-20-9713-2020

Yuan, S., Zhang, Y., Chen, J., Kang, S., Zhang, J., Feng, X., et al. (2015). Large variation of mercury isotope composition during a single precipitation event at Lhasa City, Tibetan Plateau, China. In R. Millot, & P. Negrel (Eds.), *11th applied isotope geochemistry conference aig-11* (pp. 282–286). Elsevier Science Bv. https://doi.org/10.1016/j.proeps.2015.07.066

Zheng, W., Foucher, D., & Hintelmann, H. (2007). Mercury isotope fractionation during volatilization of Hg (0) from solution into the gas phase. *Journal of Analytical Atomic Spectrometry*, *22*(9), 1097–1104. https://doi.org/10.1039/b705677j

Zheng, W., & Hintelmann, H. (2009). Mercury isotope fractionation during photoreduction in natural water is controlled by its Hg/DOC ratio. *Geochimica et Cosmochimica Acta*, *73*(22), 6704–6715. https://doi.org/10.1016/j.gca.2009.08.016

Zheng, W., & Hintelmann, H. (2010). Isotope fractionation of mercury during its photochemical reduction by low-molecular-weight organic compounds. *Journal of Physical Chemistry A*, *114*(12), 4246–4253. https://doi.org/10.1021/jp9111348

Zheng, W., Liang, L., & Gu, B. (2012). Mercury reduction and oxidation by reduced natural organic matter in anoxic environments. *Environmental Science & Technology*, *46*(1), 292–299. https://doi.org/10.1021/es203402p